Atomic Tungsten for Ultrafast Hard X-ray Generation

ARTICLE *in* THE JOURNAL OF PHYSICAL CHEMISTRY A · JUNE 2005

Impact Factor: 2.69 · DOI: 10.1021/jp0511810 · Source: PubMed

3 AUTHORS, INCLUDING:

Vernon A Couch
California Polytechnic State University, San L…
8 PUBLICATIONS **55** CITATIONS

SEE PROFILE

ARTICLES

Atomic Tungsten for Ultrafast Hard X-ray Generation

Fang Shan, Vernon A. Couch, and Ting Guo*

Department of Chemistry, University of California, One Shields Avenue, Davis, California 95616

Received: March 7, 2005; In Final Form: March 30, 2005

High-resolution X-ray absorption measurements (with an accuracy of ±0.3 eV) of $ZnSO_4$ (aq) were performed with ultrafast selected energy X-ray absorption spectroscopy (USEXAS) using a laser-driven tungsten target X-ray source. The results were used to determine the absolute spectral positions of characteristic emission lines. By comparing these positions to those predicted for the line emission from tungsten of different oxidation states using the Dirac−Fock formula, the tungsten species responsible for ultrafast hard X-ray generation were found to be tungsten atoms. This finding provides the first direct evidence to support the mechanism of X-ray generation via high-energy electrons interacting with tungsten atoms in the solid target.

I. Introduction

Ultrafast characteristic and continuum hard X-rays (a few keV to a hundred keV) have been generated with high-intensity lasers,[1−5] and these X-rays have been used in ultrafast X-ray absorption and diffraction experiments.[5−13] Many studies have been carried out to investigate hard X-ray generation mechanisms.[14,15] Although solid density targets are normally used, it has been generally considered that ultrafast hard X-rays are emitted via interactions of electrons accelerated outside the solid region of the targets with the solid material in the targets.[3,16] In contrast, less energetic X-ray radiation (<1 keV) is considered to be generated from highly charged ions in a hot plasma target.[17]

The ultrafast hard X-rays are regarded to be generated through a two-step process.[2,3,18] In the first step, intense ultrafast laser pulses interact with electrons in a less-than-solid-density plasma (produced by prepulses and pedestals) to effectively couple the photon energy to the electrons in the plasma. As a result, these electrons are greatly accelerated. In the second step of this X-ray production process, the fast electrons interact with room-temperature atoms in the target to generate X-rays, just as X-rays are generated in the conventional X-ray tubes in which both characteristic and bremsstrahlung hard X-rays are produced by electron bombardment of the solid/liquid target.[19] If this proposed model is correct, then the characteristic emission spectra from those laser-driven X-ray sources should be identical to those from the X-ray tubes, and the chemical shift or oxidation state of these X-ray emitting tungsten species should be zero. Although the magnitude of chemical shifts (the change in energy of an atomic orbital) is generally much larger than the shifts in the line emission whose energy corresponds to the difference between two energy levels, the emission spectra are easier to measure.

To date, only energy-calibrated low-resolution or noncalibrated high-resolution absorption spectra were obtained, and energy-calibrated high spectral resolution spectra that can be used to directly reveal the chemical shift or similar parameters of the X-ray emitting elements are not yet available.[3,20−23] To directly determine the hard X-ray generation mechanisms, high-resolution calibrated X-ray emission spectra from ultrafast X-ray sources are needed.

In this report, we will address this important issue by measuring the shift in the characteristic line emission with a new method developed recently in our lab, that is, ultrafast selected energy X-ray absorption spectroscopy (USEXAS). This method uses characteristic X-ray radiation of certain elements to obtain X-ray absorption spectra of others.[24,25] Since the absorption edge of an element in a compound is independent of the edge-measuring X-ray sources, the characteristic spectra used for obtaining the absorption edge can be calibrated by the measured edge. This self-referencing feature of USEXAS allows us to accurately determine the peak positions of the characteristic emission spectra. The peak positions, which equal the energy differences between two levels or edges of the characteristic emission spectra, can then be used to determine the oxidation state. As a result, USEXAS can be used to effectively study the oxidation state and thus the X-ray generation mechanisms.

We recently measured the absorption edges of several Ni compounds using USEXAS to determine the positions of L_α lines.[26] In the following, we will present the results of the absorption edge measurements of Zn in $ZnSO_4$, which can be used to more accurately measure the line positions of L_β lines that are much more sensitive to the change of oxidation state of tungsten. By comparing these results to the values obtained from theoretical studies, we can conclusively determine the oxidation states of tungsten responsible for ultrafast hard X-ray generation.

II. Experimental Section

II.1 Experimental Setup. Our laser and X-ray systems were described elsewhere.[27] The overall experimental setup is shown in Figure 1. In brief, the laser beam (30-mm diameter ($1/e^2$),

* Corresponding author. Phone: (530) 754−5283; fax: (530) 752−8995; e-mail: tguo@ucdavis.edu.

10.1021/jp0511810 CCC: $30.25
Published on Web 04/26/2005

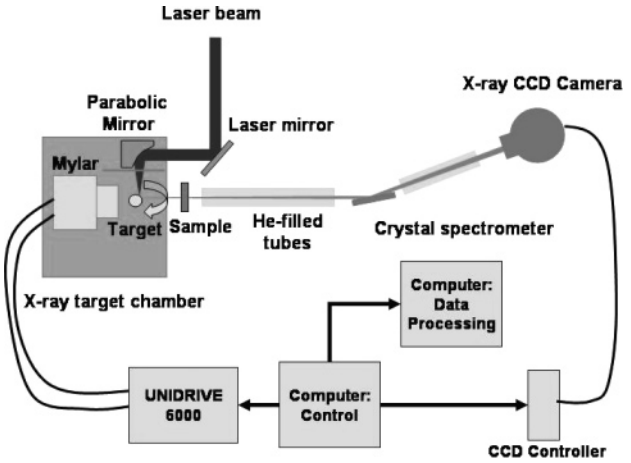

Figure 1. Experimental layout for ultrafast X-ray generation and X-ray absorption measurements.

30-fs pulse duration (shortest), 45−55 mJ per pulse at 800-nm central wavelength, and 50-Hz repetition rate) was split into two beams, one with 90% of the energy and the other 10%. The 90% beam was directed into an X-ray target chamber, in which the beam was focused by a parabolic mirror (Janos A8037-274) onto a moving tungsten rod ($^3/_8$ in. diameter, 10 in. long) target. The tungsten rod moved downward and rotated simultaneously by a step motor-driven linear stage and a second step motor. The speeds were controlled by the two step motors that were driven by an ESP6000 controller (UNIDRIVE 6000, Newport). A Labview program controlled the ESP6000. All components were controlled by a computer. A moving Mylar film (transmission 85% at 800 nm) was used to prevent the debris from reaching the parabola. The grating separation of the compressor was optimized to produce the most intense characteristic radiation of tungsten, which resulted in a lengthened pulse duration to ~1 picosecond. At this duration, the peak laser intensity was reduced from the peak intensity of $\sim 2 \times 10^{18}$ to 5×10^{16} W cm^{-2}, assuming a 10-μm diameter focal spot size.

Si(111) and GaAs(111) single crystals were used to diffract or disperse X-rays onto an LN_2 cooled, deep depletion CCD detector (Roper Scientific, PI-LCX 576). The majority of the X-ray beam path was in He-purged tubes to reduce absorption by air. The camera-target distance was 110 cm.

II.2 Samples. $ZnSO_4$ ($ZnSO_4 \cdot 7H_2O$ from Aldrich, 0.25 M) aqueous solution was prepared, and it was contained in a thin wall glass capillary (2-mm diameter, 10-μm wall thickness, Charles-Supper Company). The capillary was positioned right outside the X-ray chamber, and its position was aligned with X-rays. Zn in the sample was equivalent to a 4.5-μm bulk Zn.

II.3 Absorption Data Processing and Error Analysis. Absorption data was processed in situ with a Matlab program on a separate computer that was interfaced with the computer controlling the X-ray CCD camera, ESP6000, and step motors. Such automation was necessary for long data acquisition times, as the laser system, X-ray target, and data collection system were routinely operated for 36−48 consecutive hours.

Over a few thousand individual data files of diffraction patterns were acquired for each absorption measurement. Each diffraction data file acquired by the X-ray CCD contained a 2-D matrix. The column position corresponded to X-ray energy. For X-ray diffraction data using the tungsten target without the sample in the beam path, the theoretical values were assigned to the columns of the centroid of the diffraction lines.[28] On the basis of these assignments, the rest of the columns were

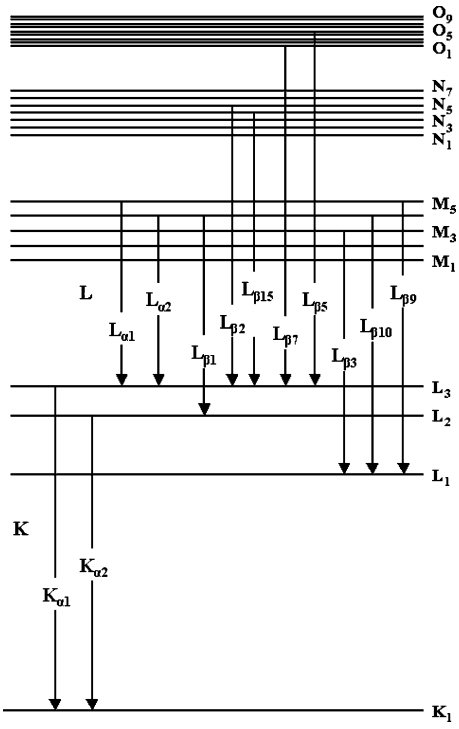

Figure 2. Energy level and transition diagram of tungsten.

transformed into their corresponding energies via the diffraction formula. After background subtraction, multiple-hits correction, and Si escape peak recalibration, the counts in the rows were summed. All the processed diffraction files were then summed to obtain the total X-ray intensity ($I_0(E)$, E is the photon energy). A similar process was used to obtain the X-ray intensity profile with the X-rays passing through the sample ($I(E)$) with the energy calibration obtained from processing the diffraction profile of I_0. The absorbance of the sample was calculated on the basis of $A(E) = -\ln(I(E)/I_0(E))$.

The experimental error in determining the X-ray absorption edge was evaluated by first employing a photon-counting noise with a Gaussian distribution to the model measured absorption data. This noise was then propagated to the first derivatives that were used for edge determination. The final error was estimated to be ±0.3 eV.

II.4 Characteristic Emission Calculations. The ground-state energy and associated eigenvalues were calculated for atomic tungsten at several ionization states (or oxidation states) by solving the Dirac−Fock equation using the program Dirac.[29] The unaltered Coulomb−Dirac Hamiltonian was used without employing fermion symmetry. The Dirac program utilizes an averaging of states method for open-shell calculations, thus giving a more complete description of the electronic structure than a single spin configuration. At lower ionization states, a single open shell was used to describe the 6s and 5d shells allowing the maximum number of configurations to be averaged (6 electrons in 12 spinors vs 4 electrons in 10 spinors), except for W(+6) which was treated as a closed shell. For oxidation states 7−9, all configurations of the 5p and 4f shells were similarly allowed.

III. Results and Discussions

The energy diagram of tungsten is shown in Figure 2. The energy levels and transitions are labeled. The energy shifts of the peak positions of characteristic emission spectra of tungsten at different oxidation states were calculated using the Dirac−

TABLE 1: Theoretically Predicted Line Emission from Tungsten as a Function of the Oxidation State[a]

	ionization stage	$L_{\beta1}$ (eV)	$L_{\beta2}$ (eV)	$L_{\beta3}$ (eV)	$L_{\alpha2}$ (eV)	$L_{\alpha1}$ (eV)	$L_{\beta5}$ (eV)	L_9 (eV)
1	our calculation	0.00	0.00	0.00	0.01	0.01	1.82	0.01
	literature	0.00	0.00	−0.01	0.00	0.00	1.79	
2	our calculation	0.01	0.00	0.00	0.01	0.01	2.56	0.04
	literature	0.02	0.03	0.01	0.01	0.01	2.86	
3	our calculation	0.07	0.09	0.06	0.08	0.07	5.72	0.11
	literature	0.12	0.16	0.11	0.11	0.12	6.28	
4	our calculation	0.18	0.27	0.17	0.19	0.18	9.42	0.22
	literature	0.27	0.36	0.28	0.25	0.26	10.13	
5	our calculation	0.34	0.55	0.34	0.35	0.35	13.61	0.36
	literature	−0.52	0.68	0.47	0.45	0.47	14.72	
6	our calculation	0.55	0.94	0.56	0.56	0.56		0.55
	literature	0.76	1.12	0.74	0.71	0.73		
7	our calculation	−0.10	2.32	−0.08	−0.02	−0.04		−0.01
	literature	−0.48	3.07	−0.36	−0.40	−0.39		
8	our calculation	−0.76	4.02	−0.73	−0.59	0.64		−0.56
	literature	−1.81	5.56	−1.51	−1.58	−1.6		
9	our calculation	−1.43	6.08	−1.38	−1.18	−1.26		−1.11
	literature	−3.21	8.63	−2.69	−2.82	−2.85		

[a] The change in the position is with respect to the neutral atom. Also shown are the literature values by Zschornack et al. Units are in eV.

Fock formula, and the results are listed in Table 1. Also listed in Table 1 are results calculated using a similar method by Zschornack et al.[31] A general agreement between our results and the literature values is evident, except for the results on $L_{\beta1}$ at oxidation state +5 and $L_{\alpha1}$ at oxidation state +8. Our results showed a positive shift for both lines at oxidation state +5 and +8, whereas the literature values remained negative.

There is also a general agreement between the calculated values and the measured shifts. For example, Khyzhun et al. and Vishnoi et al. measured the L_{III} edge shifts of tungsten in WO_3.[32,33] McGuire et al. measured the edge shift for N_V.[34] Using these results on the edges, the shifts in the peak positions of those characteristic spectra can be derived. The agreement among these three studies given here for the determination of the line shifts for $L_{\beta2}$ is good, which are 1.4 eV (using the data from Vishnoi et al. and McGuire et al.), 0.94 eV (our calculation), and 1.12 eV (calculated by Zschornack et al.), respectively.

Although previously measured Ni edge and L_α lines had been used to determine the tungsten species in the X-ray source to be at +5 or lower oxidation states, it was impossible to conclude whether the emission of ultrafast hard X-rays was from tungsten atoms or cations because the shifts in the positions for the low oxidation states (+1 to +5) are generally small, about 300 meV.[35] In this work, characteristic emission spectra involving N ($L_{\beta2}$) and O ($L_{\beta5}$) levels were used to further assess the chemical environment of the tungsten in the target during X-ray generation.

The intensities of the diffracted lines of tungsten were measured with the crystal spectrometers and the CCD, similar to the detection of Cu X-rays reported earlier.[3,27] The highest flux of W $L_{\alpha1}$ and $L_{\alpha2}$ was 6×10^{10} photons/(4π Sr sec), and the total energy conversion efficiency was 5×10^{-5} after correction of losses. The laser peak intensity was $\sim 5 \times 10^{16}$ W/cm^2, and the pulse duration was ~1000 fs. The laser focal spot size was minimized.

X-ray emission was measured with the X-ray CCD via both direct imaging mode and diffraction with single crystals. The results showed that the yields measured in the direct and diffracted modes for GaAs(111) (Virginia Semiconductor) were similar, which were close to 100%, and the diffraction efficiency for Si(111) single crystals (Czochralski, undoped, Virginia Semiconductor and Frozen zone, B-doped, Valley Design) was

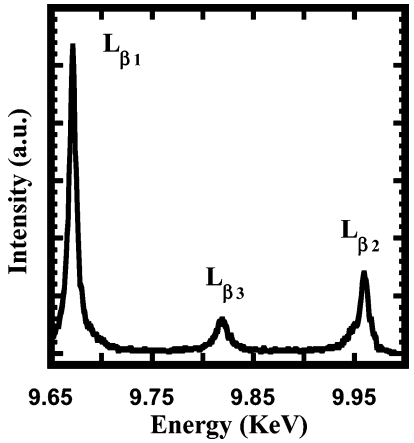

Figure 3. X-ray emission lines from the tungsten target. It shows the L_β lines. Theoretical values (listed in Table 1) are used for the positions of the centroids of these lines.

TABLE 2: X-ray Emission Lines and Line Widths from Our Tungsten Target and Literature Values[a]

	USEXAS	literature	ref
$L_{\alpha1}$	8397.0(100)	8397.6(100)	28,34
$L_{\alpha2}$	8335.0(11)	8335.2(11)	28,34
$L_{\beta1}$[b]	9672.0(67)	9672.4(67)	28,34
$L_{\beta2}$	9961.5(21)	9961.5(21)	28,34
$L_{\beta3}$	9819.0(11)	9818.8(10)	28,34
FWHM $L_{\alpha1}$	7.99 ± 0.03	6.61 ± 0.28	30, 31
FWHM $L_{\alpha2}$	8.02 ± 0.23	6.68 ± 0.39	30, 31
FWHM $L_{\beta1}$	8.67 ± 0.07	7.33 ± 0.3	30, 31
FWHM $L_{\beta2}$	10.08 ± 0.31	9.26 ± 0.93	30, 31
FWHM $L_{\beta3}$	13.61 ± 0.86	12.6 ± 1.26	30, 31

[a] FWHM (obtained from Lorentzian fits to the experimental data) and the relative intensities (in parentheses) are shown. The units for energy and FWHM are in eV and unitless for the relative intensities. [b] The intensity of $L_{\beta1}$ is set to be 67 with reference to the intensity of $L_{\alpha1}$ of 100.

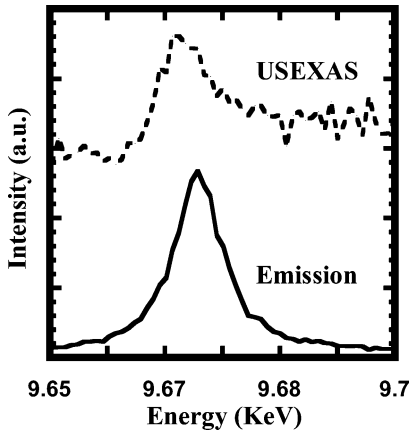

Figure 4. USEXAS data (dashed line) of $ZnSO_4$ (aq) and the $L_{\beta1}$ line.

~50% of that of the GaAs crystal. These results were similar to the literature values.[30] Unfortunately, the GaAs crystal produced lower energy resolution USEXAS spectra. Therefore, Si(111) was used to obtain all the data shown here.

The results of characteristic emission spectra measured with the crystal spectrometer in this work are shown in Figure 3 and Table 2. The diffracted profiles from Si(111) were normalized. $L_{\beta15}$ can be clearly seen as a shoulder to the left of $L_{\beta2}$. The absolute position of $L_{\beta1}$ was calibrated with the Zn edge measured with USEXAS, shown in Figure 4. The measured edge position (9664.3 eV) was very close to the literature value of Zn edge (9664.0 eV).[36] Because of the high spectral fidelity of

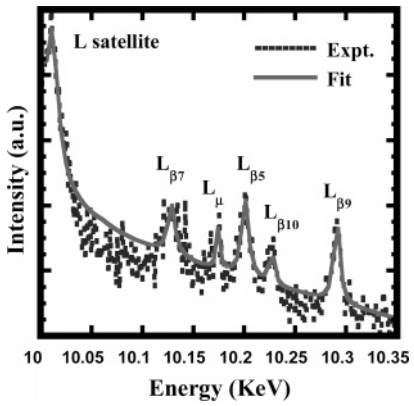

Figure 5. Measured and fitted L_β lines. The spectrum was calibrated using $L_{\beta 2}$ and $L_{\beta 9}$. Fitted parameters are listed in Table 3.

the spectrometer, the peak positions of $L_{\beta 2}$ ($L_{III}-N_V$ transition) and $L_{\beta 3}$ (L_I-M_{III} transition) were also calibrated.

The centroids of these characteristic radiation spectra are listed in Table 2. Also listed in Table are the information on L_α lines and the theoretical or literature values of the line widths and positions of the centroids from which the measured emission spectra were calibrated.[37,38] The measured full widths at half-maximum (fwhm) of these characteristic spectra were obtained by directly fitting the experimental diffraction profiles with Lorentzian X-ray emission profiles of unknown line widths. When the crystal broadening factor was included, which was estimated to be ~0.4 eV for $L_{\alpha 1}$ that was measured by the Si-(111) crystal, experimental diffraction profiles could be reproduced using the theoretical line widths and an X-ray source size of 50 μm.[39,40] Hence, most of the experimental broadening was caused by the finite source size of the X-ray target. Eeven though the literature values were used to obtain the positions of $L_{\beta 1}$ and $L_{\beta 2}$, the fact that the position of $L_{\beta 3}$ was correctly obtained confirmed that the spectrometer was correctly calibrated over the energy range of 9660−10000 eV. The measured and literature line intensities are listed in Table 2 (given in parentheses).[41,42] There is a generally good agreement between the two sets of data.

On the basis of the small shift (<0.3 eV) for the measured $L_{\beta 2}$ line emission and the calculated shifts at different oxidation states, we conclude that the oxidation states of tungsten during X-ray generation must be less than +6. Because the line emission positions were calibrated with the Zn absorption edge to be within 0.3 eV of tungsten atoms, we further conclude that the oxidation states have to be less than +4. However, as Table 1 shows, it is difficult to use the peak position of L_α and $L_{\beta 1-3}$ lines to differentiate neutral atoms from ions of +1 to +4 oxidation states, because of the small shifts between them (~150 meV).

$L_{\beta 5}$, on the other hand, is much more sensitive to the changing oxidation state, as shown in Table 1. We thus measured several other L_β lines, although their intensities were much weaker (1/200 of $L_{\beta 1}$). Figure 5 shows the results. The error in determining those line positions was less than 1 eV. We used $L_{\beta 2}$ and $L_{\beta 9}$ to calibrate other lines because these two lines are very close to those emitting from tungsten atoms when the oxidation state is between 0 and +4 (Table 1). Since we already determined that the oxidation state was below +4, it is reasonable to assume that their positions were almost identical to those of tungsten atoms. As a result, other line positions were not only obtained with high-energy resolution, but their absolute positions were calibrated. The satellite of $L_{\beta 2}$ is clearly visible. The fitted spectral profiles are shown in Figure 5, and their parameters are listed in Table 3. As shown in Table 3, the fitted $L_{\beta 5}$ is almost identical to that of atoms. Comparing to the calculated shift of ~2 eV for $L_{\beta 5}$ at oxidation +1, we conclude that the X-ray emitting species must be tungsten atoms.

TABLE 3: Fitted X-ray Emission Parameters for $L_{\beta 5}$, $L_{\beta 7}$, L_μ, and $L_{\beta 10}$[a]

	our measurement	literature[28]
$L_{\beta 9}$	10290.8	10290.7
$L_{\beta 10}$	10227.2	10227.9
$L_{\beta 5}$	10200.6	10200.4
$L\mu$	10173.2	10173.3
$L_{\beta 7}$	10128.4	10129.2
$L_{\beta 2}$ satellite	10012.1	10012.62[43]
$L_{\beta 15}$ satellite		10012.09[43]
$L_{\beta 2}$	9961.5	9961.5
$L_{\beta 15}$	9947.8	9947.8

[a] The atomic spectral positions for $L_{\beta 2}$ and $L_{\beta 9}$ were used to calibrate the positions of these four lines. The units are in eV.

Measurements on the tungsten L lines from laser-driven X-ray sources were carried out by other groups, but the spectral resolution in those measurements was low. For instance, Hironaka et al. measured the position of $L_{\alpha 1}$ to be 8.51 ± 0.12 keV.[21] Fujimoto et al. measured the position with a 100-eV shift using CCD.[20] Other line emission data from other elements were obtained, but none of the spectra was energy-calibrated. Prior to this work, the highest resolution data available was on vanadium K_α lines obtained with a Von Hamos crystal spectrometer without absolute energy calibration. Those measured peak positions were 6−8 eV below the theoretical values.[39] It was unclear whether the difference was caused by the experimental error or the Stark shift or other effects.[40,44,45]

The confirmed peak position of tungsten $L_{\beta 5}$ from the laser-driven X-ray source provides the clearest direct evidence that indicates that the X-rays are generated as the result of electrons interacting with the neutral atoms in the tungsten target and are not produced from highly ionized ions, as the Stark shifts and broadening will alter the emission profiles. As a result, one can use this mechanism to predict the yield of hard X-ray generation and to develop better schemes to generate hard X-rays.

IV. Conclusion

Using the self-referencing feature of USEXAS made possible by the presence of both the characteristic lines and the known absorption edges of compounds in the same X-ray absorption spectra, we have determined the peak positions of characteristic emission spectra from ultrafast X-ray sources in the hard X-ray region with high-energy resolution. By comparing these line positions to theoretically predicted values as a function of oxidation state, the tungsten species emitting hard X-rays were determined to be tungsten atoms.

Acknowledgment. We thank the National Science Foundation (CHE 0135132) for the financial support.

References and Notes

(1) Kieffer, J. C.; Chaker, M.; Matte, J. P.; Pepin, H.; Cote, C. Y.; Beaudoin, Y.; Johnston, T. W.; Chien, C. Y.; Coe, S.; Mourou, G.; Peyrusse, O. *Phys. Fluids B* **1993**, 5, 2676.

(2) Rousse, A.; Audebert, P.; Geindre, J. P.; Fallies, F.; Gauthier, J. C.; Mysyrowicz, A.; Grillon, G.; Antonetti, A. *Phys. Rev. E* **1994**, *50*, 2200.

(3) Guo, T.; Spielmann, C.; Walker, B. C.; Barty, C. P. J. *Rev. Sci. Instrum.* **2001**, *72*, 41.

(4) Perry, M. D.; Mourou, G. *Science* **1994**, *264*, 917.

(5) Forget, P.; Dorchies, F.; Kieffer, J. C.; Peyrusse, O. *Chem. Phys.* **2004**, *299*, 259.
(6) Guo, T.; Rose-Petruck, C.; Jimenez, R.; Raski, F.; Squier, J.; Walker, B. C.; Wilson, K. R.; Barty, C. P. J. *Picosecond-milliangstrom resolution dynamics by ultrafast X-ray diffraction*, SPIE, San Siego, CA, 1997.
(7) Guo, T.; Rose-Petruck, C.; Jimenez, R.; Raski, F.; Squier, J. A.; Walker, B. C.; Wilson, K. R.; Barty, J. P. C. *MRS Symp. Proc.* **1998**, *502*, 77.
(8) Rischel, C.; Rousse, A.; Uschmann, I.; Albouy, P. A.; Geindre, J. P.; Audebert, P.; Gauthier, J. C.; Forster, E.; Martin, J. L.; Antonetti, A. *Nature* **1997**, *390*, 490.
(9) Rose-Petruck, C.; Jimenez, R.; Guo, T.; Cavalleri, A.; Siders, C. W.; Raksi, F.; Squier, J. A.; Walker, B. C.; Wilson, K. R.; Barty, C. P. J. *Nature* **1999**, *398*, 310.
(10) Rousse, A.; Rischel, C.; Fourmaux, S.; Uschmann, I.; Forster, E.; Audebert, P.; Geindre, J. P.; Gauthier, J. C.; Hulin, D. *Meas. Sci. Technol.* **2001**, *12*, 1841.
(11) Raksi, F.; Wilson, K. R.; Jiang, Z. M.; Ikhlef, A.; Cote, C. Y.; Kieffer, J. C. *J. Chem. Phys.* **1996**, *104*, 6066.
(12) Tomov, I. V.; Rentzepis, P. M. *Chem. Phys.* **2004**, *299*, 203.
(13) Eason, R. W.; Bradley, D. K.; Kilkenny, J. D.; Greaves, G. N. *J. Phys. C: Solid State Phys.* **1984**, *17*, 5067.
(14) Wilks, S. C. *Phys. Fluids B* **1993**, *5*, 2603.
(15) Kruer, W. L. *The physics of Laser Plasma Interactions*; Addison-Wesley: New York, 1988.
(16) Chen, L. M.; Forget, P.; Fourmaux, S.; Kieffer, J. C.; Krol, A.; Chamberlain, C. C.; Hou, B. X.; Nees, J.; Mourou, G. *Phys. Plasmas* **2004**, *11*, 4439.
(17) Murnane, M. M.; Kapteyn, H. C.; Rosen, M. D.; Falcone, R. W. *Science* **1991**, *251*, 531.
(18) Kieffer, J. C.; Chien, C. Y.; Dorchies, F.; Forget, P.; Gallant, P.; Jiang, Z. M.; Pepin, H. *C. R. Acad. Sci., Ser. IV: Phys., Astrophys.* **2000**, *1*, 297.
(19) Agarwal, B. K. *X-ray Spectroscopy*, 2nd ed.; Springer-Verlag: New York, 1991; Vol. 15.
(20) Fujimoto, Y.; Hironaka, Y.; Nakamura, K. G.; Kondo, K.; Yoshida, M.; Ohtani, M.; Tsunemi, H. *Jpn. J. Appl. Phys., Part 1* **1999**, *38*, 6754.
(21) Hironaka, Y.; Inoue, T.; Fujimoto, Y.; Nakamura, K. G.; Kondo, K.; Yoshida, M. *Jpn. J. Appl. Phys., Part 2* **1999**, *38*, L242.
(22) Chen, L. M.; Forget, P.; Toth, R.; Kieffer, J. C.; Krol, A.; Chamberlain, C. C.; Hou, B. X.; Nees, J.; Mourou, G. *Rev. Sci. Instrum.* **2003**, *74*, 5035.
(23) Hagedorn, M.; Kutzner, J.; Tsilimis, G.; Zacharias, H. *Appl. Phys. B* **2003**, *77*, 49.
(24) Cheng, G.; Shan, F.; Freyer, A.; Guo, T. Ultrafast X-ray Absorption Spectroscopy using Laser Driven Electron X-ray Sources (LEXS). *Applications of X-rays Generated from Lasers and Other Bright Sources II*; San Diego, CA, 2001.
(25) Shan, F.; Carter, J. D.; Ng, V.; Guo, T. *Proc. SPIE—Int. Soc. Opt. Eng.* **2004**, *5340*, 23.
(26) Shan, F.; Carter, J. D.; Ng, V.; Guo, T. *Phys. Rev. E* **2004**, accepted.
(27) Cheng, G. J.; Shan, F.; Freyer, A.; Guo, T. *Appl. Opt.* **2002**, *41*, 5148.
(28) Bearden, J. A. *Rev. Mod. Phys.* **1967**, *39*, 86.
(29) Aa, H. J.; Jensen, T. S.; Visscher, L. *Dirac, a relativistic ab initio electronic structure program*, DIRAC04.0 ed.; 2004.
(30) Auther, A. *Dynamic theory of X-ray diffraction*; Oxford: New York, 2001.
(31) Zschornack, G.; Musiol, G.; Wagner, W. *Kernforsch., Rossendorf Dresden, [Ber.] ZfK* **1986**, *574*, 257.
(32) Khyzhun, O.; Solonin, Y.; Dobrovolsky, V. *J. Alloys Compd.* **2001**, *320*, 1.
(33) Vishnoi, A. D.; Sapre, V. B.; Mande, C. *J. Phys. Chem. Solids* **1991**, *52*, 921.
(34) McGuire, G. E.; Schewertzer, G. K.; Carlson, G. K.; Thomas, A. *Inorganic Chemistry* **1973**, *12*, 2450.
(35) Chang, C. L.; Chen, C. L.; Dong, C. L.; Chern, G.; Lee, J. F.; Jang, L. Y. *J. Electron Spectrosc. Relat.Phenom.* **2001**, *114*, 545.
(36) Nuzzo, S.; Meneghini, C.; Mobilioo, S.; Haas, H.; Riccio, P.; Fasano, A.; Cavatorta, P.; Morante, S. *Biophys. J.* **2002**, *83*, 3507.
(37) Salem, S. I.; Lee, P. L. *Phys. Rev. A* **1974**, *10*, 2033.
(38) Gokhale, B.; Shukla, S. N.; Srivastava, R. N. *Phys. Rev. A* **1983**, *28*, 858.
(39) Jiang, Z.; Kieffer, J. C.; Matte, J. P.; Chaker, M.; Peyrusse, O.; Gilles, D.; Korn, G.; Maksimchuk, A.; Coe, S.; Mourou, G. *Phys. Plasmas* **1995**, *2*, 1702.
(40) Workman, J.; Maksimchuk, A.; Liu, X.; Ellenberger, U.; Coe, J. S.; Chien, C. Y.; Umstadter, D. *Phys. Rev. Lett.* **1995**, *75*, 2324.
(41) Allison, S. K.; Armstrong, A. H. *Phys. Rev.* **1925**, *26*, 714.
(42) Nigam, A. N.; Mathur, R. B.; Jain, R. *J. Phys. B: Atom. Mol. Opt. Phys.* **1974**, *7*, 2489.
(43) Vlaicu, A.; Tochio, T.; Ishizuka, T.; Ohsawa, D.; Ito, Y.; Mukoyama, T.; Nisawa, A.; Shoji, T.; Yoshikado, S. *Phys. Rev. A* **1998**, *58*, 3544.
(44) Goldstein, W. H.; Zigler, A.; Burkhalter, P. G.; Nagel, D. J.; Barshalom, A.; Oreg, J.; Luk, T. S.; McPherson, A.; Rhodes, C. K. *Phys. Rev. A* **1993**, *47*, 4349.
(45) Kieffer, J. C.; Jiang, Z.; Ikhlef, A.; Cote, C. Y.; Peyrusse, O. *J. Opt. Soc. Am. B* **1996**, *13*, 132.